Progress In Electromagnetics Research C, Vol. 74, 41–49, 2017

A Dual-Port Sum-Difference Beam Antenna with Simple Structure and Very High Isolation

Zhichao Deng[1, *], Fushun Zhang[1], Min Liang[2], Yali Yao[1], and Fan Zhang[1]

Abstract—A simple dual-port sum-difference beam antenna with high isolation is proposed. A T-shaped slot is utilized to achieve both sum-difference beam pattern and high port-isolation. The slot coupling feeding structure simplifies the feeding network and avoids complicated fabrication. The proposed antenna is simulated, fabricated and measured. Experimental validations confirm that the antenna has 10-dB impedance bandwidths of 10.2% (4.82–5.33 GHz) for the sum port and 2.0% (4.95–5.05 GHz) for the difference port, respectively. In addition, high port-isolation better than 50 dB is achieved covering a wide band from 4.0 GHz to 5.5 GHz. The proposed antenna exhibits a measured peak gain of 6.3 dBi for the sum beam and a null depth better than −26 dB for the difference beam. Measured results agree well with simulated ones.

1. INTRODUCTION

Antennas with both sum and difference beams have found wide applications for monopulse radars which can realize accurate angle tracking and long range target detection [1–3]. Tracking as well as fine-tuning is inherently called for by the land-mobile or maritime satellite communication terminals to minimize the antenna pointing error to the fullest so as to avoid a degraded satellite link [4]. Additionally, sum and difference patterns can also be utilized in automotive radars to detect cars ahead [5] or RFID readers to narrow the angular extent of the interrogation zone [6].

Sum-difference beam pattern is usually realized by adding different weight vectors for an antenna array. In [7–11], newly designed comparator networks and phase-controlled antenna arrays are used, whereas the feeding networks become fairly complicated. Multiport antennas proposed in [4] and [12–15] show great potential to obtain a sum-difference beam with miniaturized geometries. A four-port folded dipole pair is presented in [4] to realize desired monopulse pattern, but additional comparator network is required. The monopulse pattern is also achieved in [12] by exciting different modes of a patch antenna. Using a dual-mode feeding network, the sum-difference beam is obtained for a four-port aluminum ring antenna [13]. [14] proposes a dual-port probe-fed slotted patch antenna, combined with a $0^\circ/180^\circ$ coupler, and the monopulse performance can be realized with a relative compact size. Mutual coupling among the ports, however, should be avoided for a multiport antenna to ensure its independent operation, which means high port-isolation is required here.

Inspired by a planar slotline Balun structure in [16], which indicates that a T-shaped slot can be seen as a phase inverter, a dual-port slot coupling antenna with high isolation is introduced in this paper. Instead of a complicated phasing network, the proposed antenna has a sandwiched structure with a slotted ground plane in the middle of the upper and lower substrates, by which the antenna can produce a sum-difference beam pattern within its impedance bandwidth. Additionally, high port-isolation is achieved by employing the new feeding geometry, namely T-shaped slot coupling structure.

Received 13 March 2017, Accepted 27 April 2017, Scheduled 13 May 2017

* Corresponding author: Zhichao Deng (dengzhichao@outlook.com).

[1] National Key Laboratory of Antennas and Microwave Technology, Xidian University, Xi'an 710071, P. R. China. [2] Avionics Department, Chinese Flight Test Establishment, Xi'an 710089, P. R. China.

With its advantages of easy fabrication, light weight and high isolation, the antenna is applicable for monopulse systems. Detailed dimensions of the proposed antenna are described. The working mechanism is analyzed, and measured radiation characteristics are presented in the following sections.

2. ANTENNA CONSTRUCTION

Multilayer technology and slot coupling feeding technology are employed in this design. The antenna, as a whole, is composed of three layers, and the specific structure and the prototype of the antenna are shown in Figure 1 and Figure 2, respectively. The antenna works as follows: a microstrip line on the bottom layer encourages T-shaped slot on the ground plane. And then energy is coupled to the radiation patches on the top layer through this slot. Finally, the energy is radiated into space. The substrates of proposed antenna shown in Figure 2 are both F4BM-2 with a relative permittivity of 2.65 and dielectric loss tangent of 0.02.

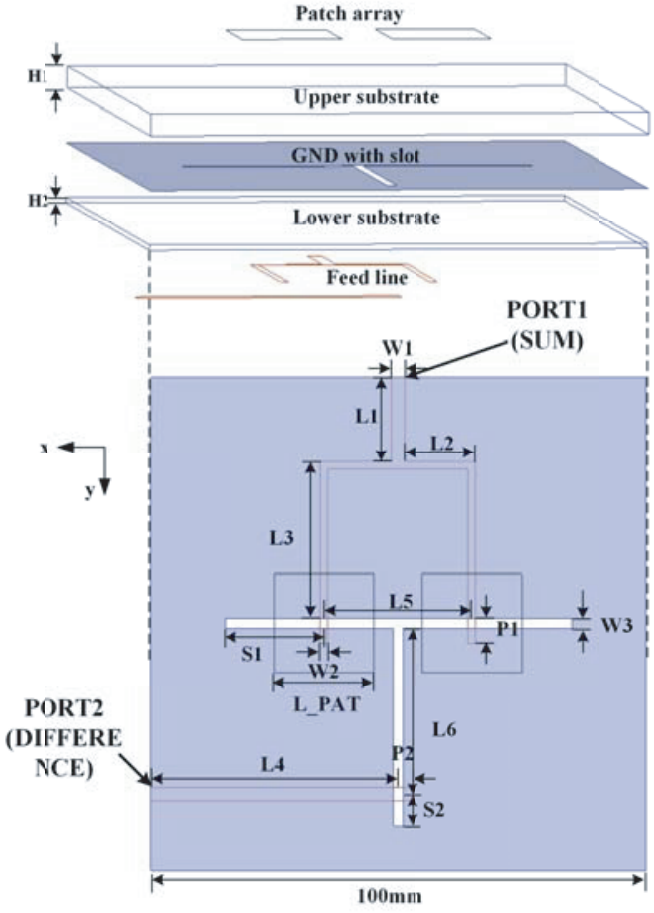

Figure 1. Configurations of the proposed antenna.

According to the transmission-line model in [17] and [18], the equivalent circuits of the feeding structure are shown in Figure 3 where the microstrip-slotline transition is modeled by an ideal transformer with a turns ratio n. Z_{om} and Z_{os} denote the characteristic impedance of the microstrip line and the slotline, respectively. Short and open stubs, as well as microstrip and slotline quarter-wave transformers, are used for impedance matching.

Using the equations in [19], turns ratio n can be calculated as follows:

$$n = \cos 2\pi \frac{h}{\lambda} u - \cot q_0 \sin 2\pi \frac{h}{\lambda} u \tag{1}$$

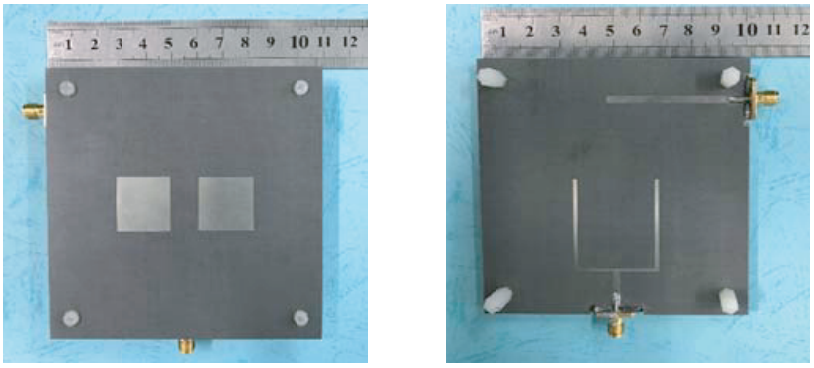

(a) (b)

Figure 2. Prototype of the proposed antenna. (a) Top view. (b) Bottom view.

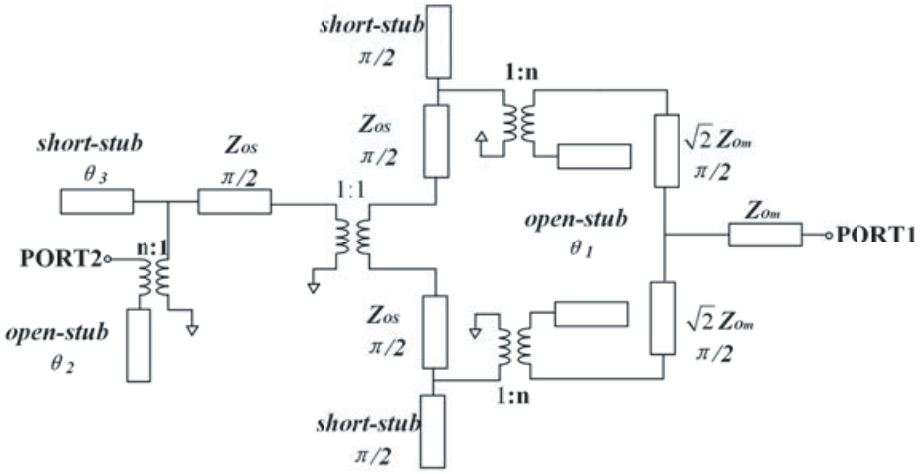

Figure 3. Equivalent circuits of the feeding structure.

where

$$q_0 = 2\pi\frac{h}{\lambda}u + \tan^{-1}\left(\frac{u}{v}\right)$$

$$u = \left[\varepsilon_r - \left(\frac{\lambda}{\lambda_s}\right)^2\right]^{1/2}$$

$$v = \left[\left(\frac{\lambda}{\lambda_s}\right)^2 - 1\right]^{1/2}$$

h is the height between the slotline and the microstrip line, λ the wavelength at the center frequency in the air and λ_s the effective wavelength at the center frequency in the slot.

Formulas in [17] can obtain the characteristic impedance Z_{om} and Z_{os}, and they are mainly decided by the widths of the microstrip line and slotline. The lengths for the two branches of the microstrip power divider and the slotline are designed to be about a quarter wavelength at around 5GHz, and influence from the patches on the impedance matching can also be fixed by adjusting the width of the slotline quarter-wave transformer. Meanwhile, the portion of the microstrip line that exceeds the slotline, having lengths of $P1$ and $P2$, can be seen as open stubs. Whereas the portion of the slotline that exceeds the microstrip line, having length of $S1$ and $S2$, can be equivalent as short stubs. By choosing appropriate n, properly adjusting the length of open and short stubs, desired impedance matching can be achieved. Through optimization, detailed parameters of the antenna are listed in Table 1.

Table 1. Optimum parameters of the proposed antenna (unit: mm).

Parameter	$L1$	$L2$	$L3$	$L4$	$L5$	$L6$	$S1$	$S2$
Value	14	15	31	50	30	34	17.5	6
Parameter	$H1$	$H2$	$W1$	$W2$	$W3$	$P1$	$P2$	L_PAT
Value	4	1	2.8	1.5	2	5	3	20

3. DISCUSSION

The T-shaped slot is not only the main element to produce the sum-difference beam, but also the core to achieve high isolation between the two ports. In this section, we will discuss the working mechanism of the T-shaped slot.

3.1. Generation of the Sum-Difference Pattern

In order to generate a sum-difference beam pattern, 0° and 180° phase differences should be achieved between the two patches. As shown in Figure 1, Port 1 is the sum port and port 2 defined as the difference port. When the sum port is excited, the energy is evenly split into two in-phase components and then coupled to the slot along the x-axis. Thus, the patches are excited in phase, and desired sum beam is obtained. On the contrary, when the difference port is excited, the energy is firstly coupled to the slot along the y-axis. The distribution of electrical field in the slot is quite similar to that in an E-plane T-junction, where the electric fields in the two branches of the slot along the x-axis are out of phase. With the phase difference of 180°, the difference beam is achieved.

The T-shaped slot can be seen as a planar E-plane T-junction, whose scattering characteristics can be described by the matrix as follow.

$$\begin{bmatrix} b_1 \\ b_2 \\ b_3 \end{bmatrix} = \frac{1}{\sqrt{2}} \begin{bmatrix} 0 & 1 & -1 \\ 1 & 0 & 0 \\ -1 & 0 & 0 \end{bmatrix} * \begin{bmatrix} a_1 \\ a_2 \\ a_3 \end{bmatrix} \tag{2}$$

In the matrix of Eq. (2), a_1, a_2, a_3 mean the incident waves, and b_1, b_2, b_3 are the reflected waves of each port. To better illustrate the port characteristics, simulated electric field distributions in the T-shaped slot are presented in Figure 4. It is well observed that when the sum port is excited, the electric fields in the two slot branches are in phase. On the other hand, when the difference port is excited, the electric fields in the two slot branches are out of phase.

3.2. Achievement of High Port-Isolation

When ports T2 and T3 in Figure 4 are excited in phase, which means that $a_2 = a_3 = 1$ and $a_1 = 0$, it can be calculated in the matrix of Eq. (2) that the output at T1 is zero. This explains the theory how we achieve high port-isolation in this design: when the sum port is excited, the two branches of the slot along the x-axis are encouraged in phase. And it is the exact condition that we just discussed above where the output at the difference port is zero. On the contrary, when the difference port is excited, the two branches of the forklike feed line are excited out of phase. As a result, the energies cancel out with each other at the fork point of the power divider, which makes the output at the sum port also zero. Figure 5 gives simulated surface current distributions of the feed line. It can be found that when one port is excited, the current distribution on the feed line of the other port is weak. This agrees with the assumption that the energy can hardly be transmitted or coupled to the other port, in which case the high isolation between the two ports can be achieved.

4. PARAMETRIC STUDY

Parameters sensitive to the design are optimized and analyzed for further studies. When one parameter is studied, the others stay constant as shown in Table 1.

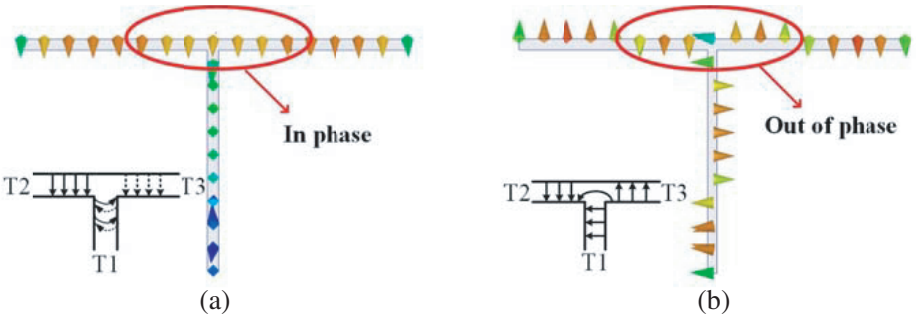

Figure 4. Electric field distributions in the T-shaped slot when (a) the sum port is excited; (b) the difference port is excited.

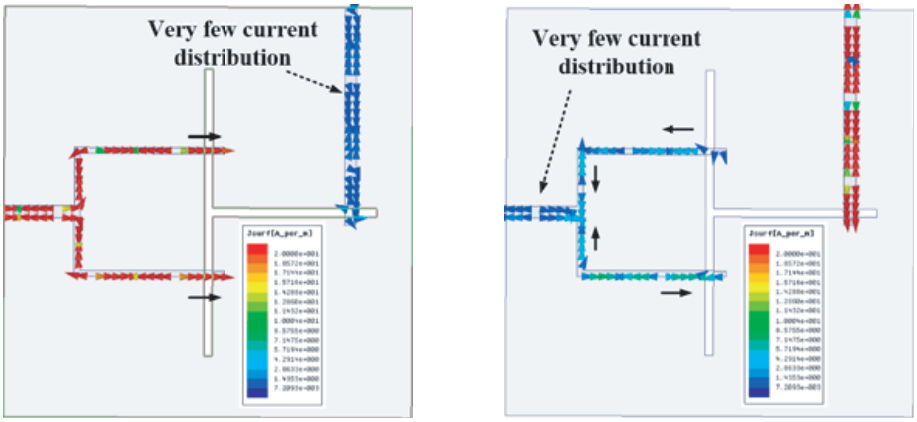

Figure 5. Surface current distribution of the feed line when (a) the sum port is excited; (b) the difference port is excited.

4.1. Effects of Length $S1$, $S2$ on the Impedance Matching

$S1$ and $S2$ are the lengths for the portion of the slot that exceed the microstrip line. This portion can be seen as short-circuited stubs, and impedance matching can be realized by adjusting the lengths of $S1$ and $S2$ properly. Figure 6 shows that impedance matching is realized for both ports when $S1$ and $S2$ are set as 17.5 mm and 6 mm, respectively. It is also noted that varying $S1$ has great effect on impedance matching for both ports, because part of $S1$ lies under the patches, and such a part has great influence on the coupling between the patches and slotline. These results can also be concluded from the equivalent circuits in Figure 3.

4.2. Effects of Length $P1$, $P2$ on the Impedance Matching

$P1$ and $P2$ are the lengths for the portion of the microstrip line that exceeds the slot. The feed lines can be seen as open-circuited stubs, and they crucially determine the reactance parts of input impedances of port 1 and port 2 [20], respectively. Figure 7 shows that impedance matching is realized when $P1$ and $P2$ are set as 5 mm and 4 mm, respectively.

4.3. Effects of Height $H1$ on the Radiation Pattern

$H1$ is the height of the upper substrate and has a great effect on the coupling degree. Additionally, different heights between the slot and the patches will cause different reflection situations, which will finally influence the antenna's radiation patterns. In Figure 8, it is found that the best null depth of the

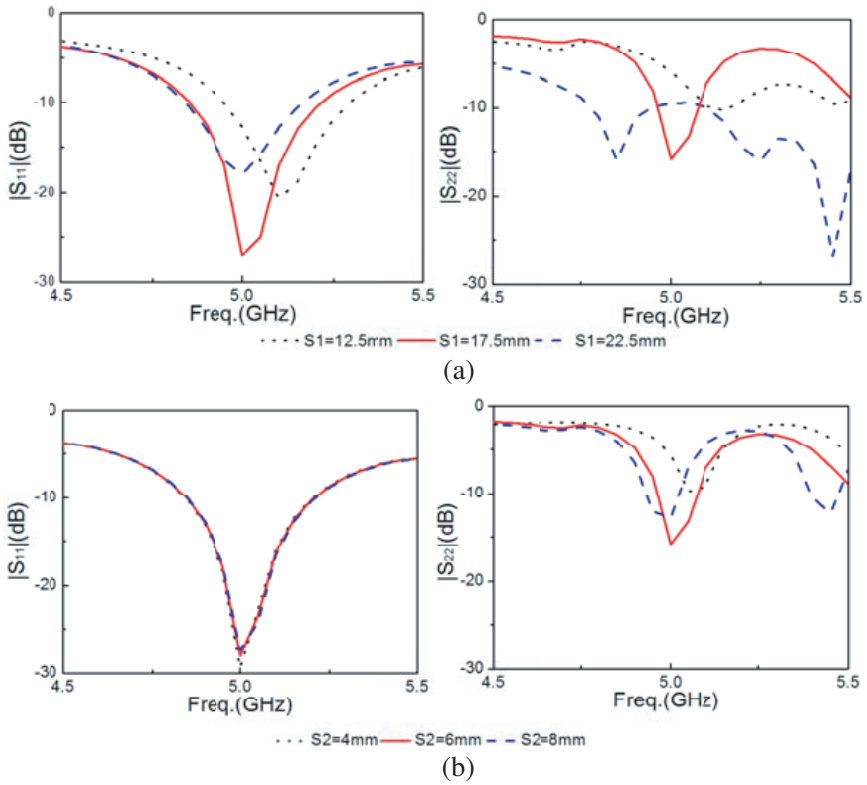

Figure 6. Simulated S-parameters with varying (a) $S1$; (b) $S2$.

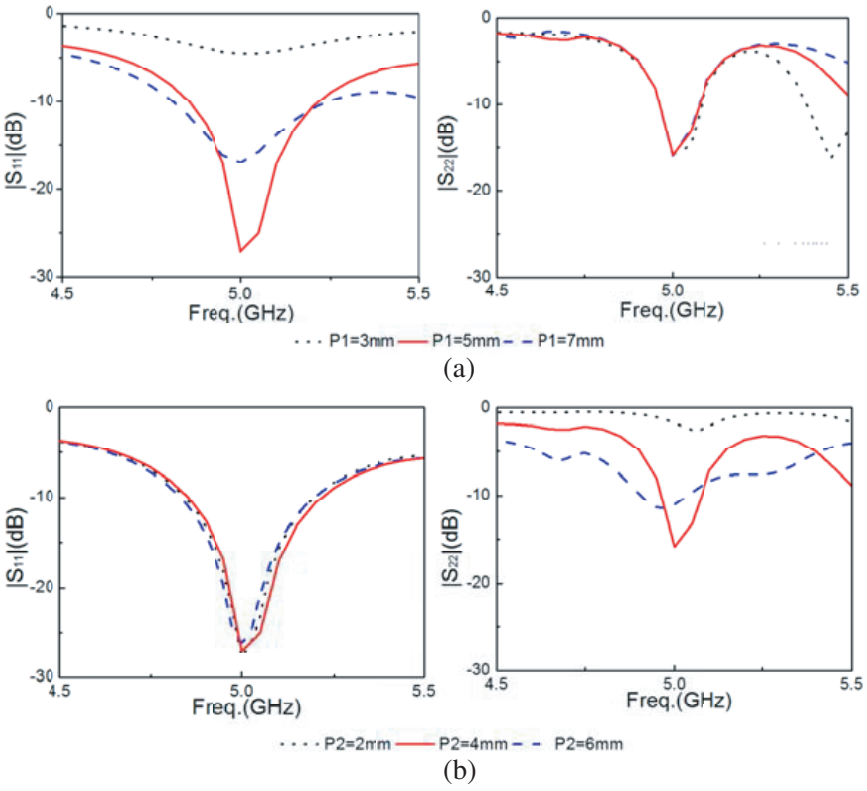

Figure 7. Simulated S-parameters with varying (a) $P1$; (b) $P2$.

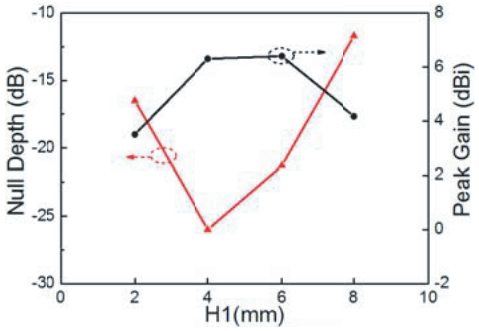

Figure 8. Simulated null depths of difference beam and peak gains of sum beam with varying $H1$.

difference beam and peak gain of the sum beam are both achieved when $H1$ is set as 4 mm. Furthermore, it is noted that when $H1$ is set as 2 mm, the peak gain of sum beam is only −1.4 dBi because the slot and patches are too close, which causes deteriorated impedance matching and backward radiation.

5. EXPERIMENTAL RESULT AND COMPARISON

Based on the studies in the previous sections, the dual-port sum-difference beam antenna proposed in this paper is fabricated and measured to validate the design.

Figure 9 gives simulated and measured S-parameters. Simulated results are obtained by ANSYS HFSS ver.15, and the measurements are carried out using the Wiltron 37269A Network Analyzer. It is shown that both the sum and difference ports resonate at 5 GHz. Impedance bandwidths of 10.2% (4.82–5.33 GHz) and 2.0% (4.95–5.05 GHz) are achieved for the sum and difference ports, respectively. Additionally, it can be seen that the isolation between port 1 and port 2 is better than 50 dB covering a wide band from 4.0 GHz to 5.5 GHz. Measured results agree with simulated ones well with acceptable differences. The manufacture errors affect the impedance of the antenna, which may lead to the disagreement between simulations and measurements.

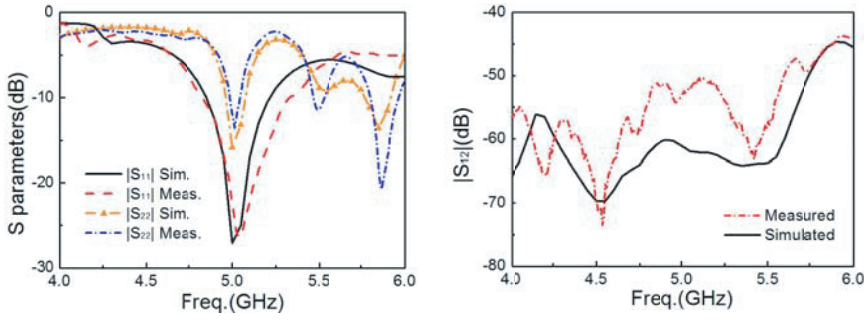

(a) (b)

Figure 9. Simulated and measured S parameters of proposed antenna. (a) Return Loss; (b) Isolation.

The proposed antenna is measured in an anechoic chamber. Simulated and measured gain patterns of the elevation plane at 5 GHz are plotted in Figure 10. It can be seen that both the sum and difference patterns are obtained, while the difference beam has a null depth better than −26 dB at the center (theta = 0°), and the sum beam has a maximum gain of 6.7 dBi with a 3-dB beam width of 50°. Normally, a two-unit array has a typical gain of 8–10 dBi. For a slot coupling structure, however, backward radiation from the slotline inevitably weakens the directivity of the antenna, which eventually leads to a decrease on the gain of the array. Simulated radiation efficiency versus frequency curves is also provided in Figure 10, which shows that the efficiencies for the sum and difference beams are both above 0.9 in the operating band. It can be further observed that the co-polar components are much stronger than the cross-polar components, which exhibits a good capability of tracking signals.

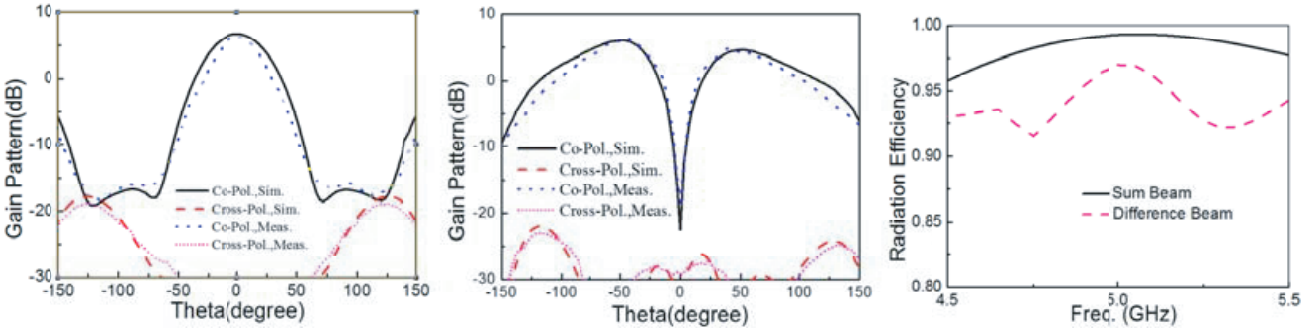

Figure 10. Gain patterns and simulated radiation efficiency.

Table 2 lists the comparisons of various sum-difference antennas. It can be seen that the proposed antenna has an outstanding port-isolation with a sum-difference beam pattern realized.

Table 2. Comparisons of various multi-port sum-difference antennas.

Reference	Operating bandwidth /Antenna size	Peak gain (dB)	Null (dB)	Isolation (dB)
[4]	1.54–1.58 GHz (2.6%) $0.68\lambda_0 \times 0.5\lambda_0 \times 0.16\lambda_0$	11	-25	≥ 20
[12]	2.40–2.48 GHz (1.5%) /	2.8	-34	≥ 30
[13]	0.96–1.7 GHz (55%) $0.71\lambda_0 \times 0.71\lambda_0 \times 0.21\lambda_0$	7.6	-10	≥ 30
[14]	2.11–2.455 GHz (15%) $0.63\lambda_0 \times 0.69\lambda_0 \times 0.11\lambda_0$	7.5	-32.7	≥ 15
[15]	1.565–1.587 GHz (1.4%) $1.05\lambda_0 \times 1.05\lambda_0 \times 0.02\lambda_0$	7.5	-30	≥ 20
This work	4.95–5.05 GHz (2.0%) $1.67\lambda_0 \times 1.67\lambda_0 \times 0.1\lambda_0$	6.3	-26	≥ 50

6. CONCLUSION

A novel and simple dual-port sum-difference beam antenna with very high isolation is proposed, fabricated and measured. The conventional feeding network with complicated power dividers is replaced by a simple T-shaped slot. The proposed antenna can produce both sum and difference beams as a result of exciting different ports. High port-isolation is also achieved to avoid interactions between the two ports. The proposed antenna has 10-dB impedance bandwidths of 10.2% (4.82–5.33 GHz) for the sum port and 2.0% (4.95–5.05 GHz) for the difference port, respectively. In addition, high port-isolation better than 50 dB is achieved covering a wide band from 4.0 GHz to 5.5 GHz. The sum-difference pattern is obtained with a measured peak gain of 6.3 dBi for the sum beam and a measured null depth better than -26 dB for the difference beam. With its sum and difference beam properties, high port-isolation, easy fabrication and light weight, the antenna is a good candidate for monopulse systems.

REFERENCES

1. Sherman, S. M. and D. K. Barton, *Monopulse Principles and Techniques*, Artech House, 1984.

2. Song, M. Z. and T. Hong, "Sum and difference multiple beam modulation transmitted by multimode horn antenna for inverse monopulse direction-finding," *Progress In Electromagnetics Research*, Vol. 82, 367–380, 2008.
3. Xu, J., et al., "Sum and difference beamforming for angle-doppler estimation with STAP-based radars," *IEEE Transactions on Aerospace and Electronic Systems*, Vol. 52, 2825–2836, Dec. 2016.
4. Yin, J., et al., "Monopulse tracking performance of multi-port eleven antenna for use in satellite communications terminals," *EuCAP 2007, The Second European Conference on Antennas and Propagation*, 2007.
5. Grimes, D. M. and C. A. Grimes, "Cradar — An open-loop extended-monopulse automotive radar," *IEEE Trans. Veh. Technol.*, Vol. 38, No. 3, 123–131, 1989.
6. Hansen, T. B. and M. L. Oristaglio, "Method for controlling the angular extent of interrogation zones in RFID," *IEEE Antennas and Wireless Propagation Letters*, 134–137, 2006.
7. Anudeep, B., "Interferometer pattern technique for antenna null synthesis," *International Conference on WiSPNET*, 1599–1602, 2016.
8. López, P., et al., "Subarray weighting for the difference patterns of monopulse antennas: Joint optimization of subarray configurations and weights," *IEEE Transactions on Antennas and Propagation*, Vol. 49, No. 11, 1606–1608, Nov. 2001.
9. Kwak, S., J. Chun, et al., "Asymmetric sum and difference beam pattern synthesis with a common weight vector," *IEEE Antennas and Wireless Propagation Letters*, Vol. 15, 1622–1625, 2016.
10. Wang, H., et al., "A compact single layer monopulse microstrip antenna array," *IEEE Transactions on Antennas and Propagation*, Vol. 54, No. 2, 2006.
11. Oliveri, G. and L. Poli, "Synthesis of monopulse sub-arrayed linear and planar array antennas with optimized sidelobes," *Progress In Electromagnetics Research*, Vol. 99, 109–129, 2009.
12. Maddio, S., "A circularly polarized switched beam antenna with pattern diversity for WiFi applications," *IEEE Antennas and Wireless Propagation Letters*, Vol. 16, 125–128, 2016.
13. Peng, H.-L., et al., "A compact single/dual-polarized broadband antenna with SUM and difference beam capabilities," *IEEE Antennas and Wireless Propagation Letters*, Vol. 9, 990–993, 2010.
14. Yu, F., et al., "Single patch antenna with monopulse patterns," *IEEE Microwave and Wireless Components Letters*, Vol. 26, No. 10, 762–764, Oct. 2016.
15. Labadie, N. R, S. K. Sharma, and G. M. Rebeiz, "A circularly polarized multiple radiating mode microstrip antenna for satellite receive applications," *IEEE Transactions on Antennas and Propagation*, Vol. 62, 3490–3500, 2012.
16. Yao, Y.-L., et al., "Planar wideband balun with novel slotline T-junction transition," *Progress In Electromagnetics Research Letters*, Vol. 64, 73–79, 2016.
17. Gupta, K. C., R. Carg, I. Bahl, and P. Bhartia, *Microstrip Lines and Slotlies*, Artech House, 1996.
18. Kim, J. P. and W. S. Park, "Novel configurations of planar multilayer magic-T using microstrip-slotline transitions," *IEEE Transactions on Microwave Theory and Techniques*, Vol. 50, No. 7, 1683–1688, Jul. 2002.
19. Knorr, J. B., "Slot-line transitions," *IEEE Transactions on Microwave Theory and Techniques*, Vol. 22, No. 5, 548–554, May 1974.
20. Sullwan, P. L. and D. H. Schaubert, "Analysis of an aperture coupled microstrip antenna," *IEEE Transactions on Antennas and Propagation*, Vol. 34, No. 8, 977–984, Aug. 1986.